ARTICLE NO. 79-0379R

Flow Computations in Inlets at Incidence Using a Shock Fitting Bicharacteristic Method

Joseph Vadyak* and Joe D. Hoffman†
Purdue University, West Lafayette, Ind.
and
Allan R. Bishop‡
NASA Lewis Research Center, Cleveland, Ohio

An analysis is presented for calculating the flowfield in supersonic mixed-compression aircraft inlets operating at angle of attack. The flowfield is computed by a steady three-dimensional bicharacteristic method. The bow shock wave and the reflected internal shock wave system are computed by a three-dimensional, discrete shock wave fitting procedure. Viscous and thermal diffusion may be included as source terms in the bicharacteristic method. A production type of computer program capable of determining the flowfield in a variety of axisymmetric mixed-compression supersonic inlets is available. The results of the present analysis agree well with those produced by the two-dimensional method of characteristics when axisymmetric flowfields are computed. For three-dimensional flowfields, the results of the present analysis agree well with experimental data except in regions of high viscous interaction and boundary-layer removal. The present analysis does not compute the boundary layer, nor does it account for boundary-layer bleed.

Nomenclature

a	= speed of sound
c	= velocity of divergence of Mach cone
F_e	= source term in the energy equation
F_x,F_y,F_z	= source terms in the x, y, and z component momentum equations
i,j,k	= unit vectors in the x, y, and z directions, respectively
n	= unit vector normal to a characteristic surface
n_b	= unit vector normal to a solid boundary surface
n_s	= unit vector normal to a shock wave surface
P	= pressure
q	= velocity magnitude
r	= radial position
t	= time
T	= temperature
u,v,w	= velocity components corresponding to x,y,z
x,y,z	= Cartesian coordinates
α	= angle of attack
α_i,β_i	= unit vectors in the bicharacteristic parameterization
θ	bicharacteristic parameterization angle, or polar
ρ	= density

Subscripts

i,j,k	= Cartesian coordinate indices (1-3)
x,y,z	= partial differential with respect to x,y,z

Introduction

THE purpose of this investigation[1] was to develop a method for calculating the flowfield in a supersonic mixed-compression inlet operating at angle of attack. A typical mixed-compression inlet is illustrated in Fig. 1. Compression takes place both in the external flow about the forebody and in the internal flow inside the annulus. Since the freestream velocity is supersonic, a bow shock wave is generated at the forebody tip. An internal shock wave emanates from the cowl lip and makes a number of reflections with the centerbody and cowl before terminating in the divergence that is downstream of the geometric throat of the annulus. The flow is subsonic downstream of that location.

The inlet illustrated in Fig. 1 is axisymmetric. At zero incidence, the flowfield is axisymmetric and can be computed using a two-dimensional method. At nonzero angle of attack, cross flow develops, and computation of the flowfield requires using a three-dimensional algorithm.

The equations of motion for steady three-dimensional supersonic flow may be classified as a system of hyperbolic quasilinear partial differential equations of first order. In the present investigation, those equations are solved numerically using the method of characteristics for steady three-dimensional flow. The bow shock wave and the internal shock wave system are computed using a three-dimensional discrete shock wave fitting procedure. The influence of molecular transport may be included in the computation by treating the viscous and thermal diffusion terms in the governing partial differential equations of motion as source terms in the method of characteristics scheme. The primary intent in including the effects of molecular transport is for the future matching of the present analysis with a higher order, three-dimensional boundary-layer analysis in a manner suggested by Ferri and Dash.[2] No attempt was made in the present investigation to compute the boundary layer, or to account for boundary-layer removal.

The shock fitting technique used in the present study divides the computational regime into regions of continuous flow, each region being bounded by solid boundary stream surfaces and discontinuities. Independent interpolations are performed on each side of a discontinuity with the difference in flow properties between the upstream and downstream sides of a given discontinuity being determined by the application of the local Hugoniot relations. This approach differs from the floating shock fitting technique originally suggested by Richtmyer and Morton[3] and later employed by Moretti[4] and Salas.[5] In the floating shock fitting techniques, the computational regime is treated as a single region in which the mesh points are typically equally spaced. Discontinuities are

Presented as Paper 79-0379 at the AIAA 17th Aerospace Sciences Meeting, New Orleans, La., Jan. 15-17, 1979; submitted Jan. 26, 1979; revision received May 9, 1980.

Index categories: Airbreathing Propulsion; Computational Methods; Supersonic and Hypersonic Flow.

*Visiting Assistant Professor of Mechanical Engineering. Member AIAA.

†Professor of Mechanical Engineering. Member AIAA.

‡Member of Aerodynamics Analysis Section, Wind Tunnel and Flight Division.

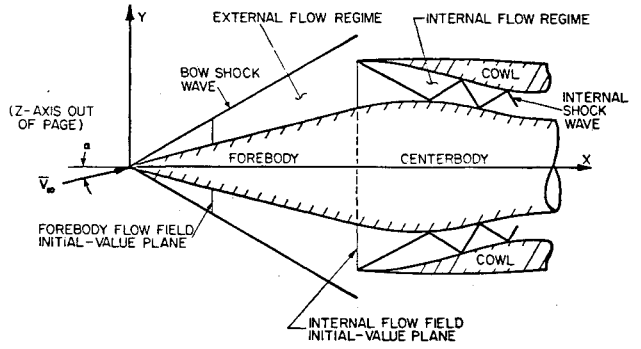

Fig. 1 Mixed-compression inlet.

then allowed to float over the fixed grid with their location and strength being determined by the governing equations. Thereby, in floating shock fitting methods, discontinuities are explicitly treated but do not, however, act as boundaries of the flow.

Gasdynamic Model

The gasdynamic model is based upon the following assumptions: steady flow, negligible body forces, a simple system in thermodynamic equilibrium, and viscous and thermal diffusion effects of secondary importance. The governing equations for the assumed flow model consist of the continuity equation, the component momentum equations, the energy equation, the thermal and caloric equations of state, and the appropriate representations for the molecular transport properties.

A major assumption of the present investigation is that the influence of molecular transport is considered to be of secondary importance as compared to the inertial effects, which are constituted by the convective terms and the pressure gradient in the governing partial differential equations of motion. As a consequence, the viscous and thermal diffusion terms appearing in the governing equations are treated as source terms in the method of characteristics scheme. In what follows, the molecular transport terms are placed on the right-hand sides of the respective governing equations, and the convective terms and pressure gradient are placed on the left-hand sides of those equations and are considered as constituting the principal parts of those equations. The characteristic surfaces of the flow are determined only by the principal parts of the governing equations.

For steady three-dimensional flow, the equations of motion are given by

$$\rho u_x + \rho v_y + \rho w_z + u\rho_x + v\rho_y + w\rho_z = 0 \tag{1}$$

$$\rho u u_x + \rho v u_y + \rho w u_z + P_x = F_x \tag{2}$$

$$\rho u v_x + \rho v v_y + \rho w v_z + P_y = F_y \tag{3}$$

$$\rho u w_x + \rho v w_y + \rho w w_z + P_z = F_z \tag{4}$$

$$uP_x + vP_y + wP_z - a^2(u\rho_x + v\rho_y + w\rho_z) = F_e \tag{5}$$

In Eqs. (2-5), the parameters F_x, F_y, and F_z denote the viscous shear stress terms in the x, y, and z component Navier-Stokes equations, respectively, and F_e denotes the molecular transport terms in the energy equation. The term F_e is composed of a thermal conduction function and a viscous heat dissipation function. The detailed representations for F_x, F_y, F_z, and F_e are given in Ref. 1.

It is assumed that the working gas may be represented as a simple system in thermodynamic equilibrium. Thus, specification of any two independent thermodynamic properties defines the thermodynamic state of the system. The pressure P and the density ρ are considered as the primary thermodynamic variables. The temperature T and the sonic speed a are expressed in terms of the primary thermodynamic variables P and ρ. The general functional forms of the relations for T and a are given by

$$T = T(P,\rho) \tag{6}$$

$$a = a(P,\rho) \tag{7}$$

The dynamic viscosity and the thermal conductivity must be expressed in terms of the primary thermodynamic variables P and ρ. They are assumed to be functions of the temperature only.

The contribution of turbulent transport may be considered by adding the appropriate eddy viscosity and eddy thermal conductivity functions to the molecular transport properties.

Characteristic Equations

Equations (1-5), with the left-hand sides constituting the principal parts, may be classified as a system of quasilinear nonhomogeneous partial differential equations of first order. The system is hyperbolic if the flow is supersonic. Systems of hyperbolic partial differential equations in three independent variables have the property that there exist surfaces in three-dimensional space on which linear combinations of the original partial differential equations can be formed that contain derivatives only in the surfaces themselves. These special surfaces are called characteristic surfaces, and the linear combinations of the original differential equations are interior differential operators known as compatibility relations.

For steady three-dimensional supersonic flow, two families of characteristic surfaces exist. One family of characteristic surfaces consists of the stream surfaces which are surfaces composed of streamlines. A streamline may be represented by

$$dx/dt = u \qquad dy/dt = v \qquad dz/dt = w \tag{8}$$

where t is the time of travel of a fluid particle along the streamline. The compatibility relations that are applicable on the stream surfaces are given by

$$\frac{dP}{dt} - a^2 \frac{d\rho}{dt} = F_e \tag{9}$$

$$\rho u \frac{du}{dt} + \rho v \frac{dv}{dt} + \rho w \frac{dw}{dt} + \frac{dP}{dt} = uF_x + vF_y + wF_z \tag{10}$$

In Eqs. (9) and (10), the operator $d(\ )/dt$ represents the directional derivative along a streamline.

The second family of characteristic surfaces consists of the wave surfaces. The envelope of all wave surfaces at a point forms a conoid known as the Mach conoid. The Mach conoid may be represented locally by a right circular cone known as the Mach cone. The line of contact between a particular wave surface and the Mach conoid is known as a bicharacteristic. Thereby, a bicharacteristic is a generator of the Mach conoid.

D. S. Butler[6] developed a parametric form for representing a bicharacteristic and the wave surface compatibility relation applicable along it. Butler's bicharacteristic parameterization is given by

$$dx_i = (u_i + c\alpha_i \cos\theta + c\beta_i \sin\theta)\,dt \qquad (i = 1,2,3) \tag{11}$$

where t is the time of travel of a fluid particle along the streamline that is the axis of the Mach cone, θ is a parametric angle denoting a particular element of the Mach cone and has

the range $0 \le \theta \le 2\pi$, and c is given by

$$c^2 = q^2 a^2 / (q^2 - a^2) \tag{12}$$

The vectors α_i and β_i in Eq. (11) are parametric unit vectors with α_i, β_i, and $u_i/q\,(i=1,2,3)$ forming an orthonormal set. The corresponding parametric form of the wave surface compatibility relation is given by

$$\frac{dP}{dt} + \rho c(\alpha_i \cos\theta + \beta_i \sin\theta)\frac{du_i}{dt} =$$

$$\Phi - \rho c^2 (\alpha_i \sin\theta - \beta_i \cos\theta)(\alpha_j \sin\theta - \beta_j \cos\theta)\frac{\partial u_i}{\partial x_j} \tag{13}$$

In Eq. (13), the operator $d(\ )/dt$ represents differentiation in the bicharacteristic direction, and Φ is given by

$$\Phi = (c^2/a^2)[F_e - a(n_x F_x + n_y F_y + n_z F_z)] \tag{14}$$

where $n = (n_x, n_y, n_z)$ denotes the unit vector normal to the wave surface, which may be written in parametric form as

$$n_i = (a/c)(cu_i/q^2 - \alpha_i \cos\theta - \beta_i \sin\theta) \qquad (i=1,2,3) \tag{15}$$

In addition to the above relations, Butler also developed a noncharacteristic relation which is applicable along a streamline. This noncharacteristic relation is given by

$$\frac{dP}{dt} = \sigma - \rho c^2 (\alpha_i \alpha_j + \beta_i \beta_j)\frac{\partial u_i}{\partial x_j} \tag{16}$$

where the operator $d(\ )/dt$ denotes differentiation along a streamline, and σ is given by

$$\sigma = (c^2/a^2)F_e - (c^2/q^2)(uF_x + vF_y + wF_z) \tag{17}$$

At any point in the flowfield there exist an infinite number of stream surfaces and wave surfaces. The number of independent compatibility relations cannot exceed the number of independent equations of motion. Consequently, it is necessary to determine which of the possible combinations of the compatibility relations form an independent set. Rusanov,[7] using a proof in the space of characteristic normals, has shown for steady three-dimensional isentropic flow that two of the stream surface compatibility relations applied along a stream surface and the single wave surface compatibility relation applied along three different wave surfaces form an independent set of five characteristic relations. Rusanov's results may be extended to the present case since the principal parts of Eqs. (1-5) are the same as those for isentropic flow.

Unit Processes

General Considerations

A variety of unit processes are employed in the computation of the flowfield. The unit processes may be classified into four major types: interior point, solid boundary point, field-shock wave point, and solid body-shock wave point. The basic interior point and solid boundary point schemes have been employed in previous investigations by Ransom, Hoffman, and Thompson[8] and Cline and Hoffman.[9] Those algorithms, however, require modifications when used in the internal flow computations when the solution point is in the vicinity of a shock wave. The field-shock wave point and solid body-shock wave point schemes were devised specifically for this investigation.

In the overall numerical algorithm, an inverse marching scheme is employed. The solution is obtained on space-like planes of constant x, where the x axis is the longitudinal axis of the centerbody and the cowl. For the internal flow, the solution is also obtained on the space curves which are defined by the intersections of the internal shock wave with the solid boundaries. Except in the vicinity of a shock wave-solid boundary intersection, the distance Δx between successive solution planes is determined by the application of the Courant-Friedrichs-Lewy (CFL) stability criterion.[10] In the vicinity of a shock wave intersection with a solid boundary, the axial distance between successive solution planes is chosen so that the entire shock wave-solid boundary intersection falls between two adjacent solution planes. The marching step Δx is determined prior to the application of the unit processes.

Interior Point and Solid Boundary Point Unit Processes

The interior point scheme is an explicit predictor-corrector algorithm, with the corrector generally being iterated to convergence. The computational network used in determining an interior point is illustrated in Fig. 2. Points 1-4 represent the intersection points of four rearward-running bicharacteristics with the initial-value plane, point 5 is the streamline intersection point with the initial-value plane, and point 6 is the solution point.

The unit process is initiated by determining the location of the solution point. The coordinates of point 6 are computed by extending the streamline from point 5 to the solution plane using the following finite-difference form of Eq. (8).

$$x_i(6) - x_i(5) = \tfrac{1}{2}[u_i(5) + u_i(6)][t(6) - t(5)]$$

$$(i=1,2,3) \tag{18}$$

Interpolated flow property values at point 5 are used in the integration, even though point 5 is a known field point. As shown by Ransom, Hoffman, and Thompson,[8] this interpolation is required to produce a stable numerical scheme. The interpolated flow property values are obtained from the following quadratic bivariate interpolation polynomial

$$f(y,z) = a_1 + a_2 y + a_3 z + a_4 yz + a_5 y^2 + a_6 z^2 \tag{19}$$

where $f(y,z)$ denotes a general function of the coordinates y and z, and the coefficients $a_i\,(i=1\text{-}6)$ are obtained from a least squares fit of nine neighboring data points in the initial-value plane.

With the location of the solution point determined, four bicharacteristics are extended from the solution point back to the initial-value plane to intersect this plane at points 1-4. The coordinates of each of these intersection points are determined using the following finite-difference form of Eq. (11)

$$x_i(6) - x_i(k) = \tfrac{1}{2}\{u_i(k) + u_i(6) + [c(k) + c(6)]$$

$$\times [\alpha_i \cos\theta(k) + \beta_i \sin\theta(k)]\}[t(6) - t(k)] \qquad (i=1,2,3) \tag{20}$$

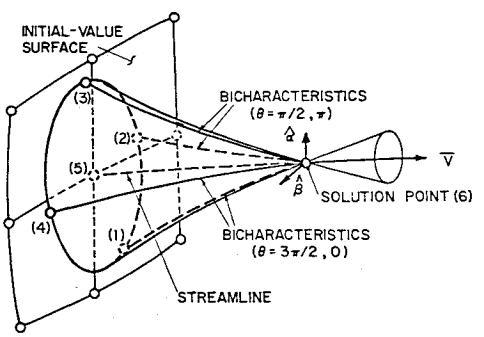

Fig. 2 Interior point computational network.

The index k in Eq. (20) denotes the bicharacteristic-initial-value plane intersection point illustrated in Fig. 2 and has a range of 1-4, corresponding to the $\theta(k)$ values of 0, $\pi/2$, π, and $3\pi/2$, respectively. The flow property values at points 1-4 are obtained by interpolation using Eq. (19).

Once the positions of and the flow properties at points 1-5 have been determined, the system of nonlinear compatibility equations, written in finite-difference form, is solved to obtain the five flow properties $u(6)$, $v(6)$, $w(6)$, $P(6)$, and $\rho(6)$. Two of the five required compatibility equations are given by Eqs. (9) and (10). These equations are written in finite-difference form by replacing the derivatives with simple differences, and by replacing the coefficients of the derivatives with the arithmetic average of the coefficients at the solution point and at the appropriate point in the initial-value plane. To obtain the remaining three required compatibility equations, appropriate linear combinations of the wave surface compatibility relation [Eq. (13)], applied along each of the four bicharacteristics, and the noncharacteristic relation [Eq. (16)], applied along the streamline, are formed. One independent linear combination of the compatibility equations is obtained by subtracting the finite-difference form of Eq. (13) evaluated for $\theta=\pi$ from the finite-difference form of Eq. (13) evaluated for $\theta=0$. Another independent linear combination is obtained by subtracting the finite-difference form of Eq. (13) evaluated for $\theta=3\pi/2$ from the finite-difference form of Eq. (13) evaluated for $\theta=\pi/2$. The final independent linear combination is obtained by subtracting the finite-difference form of the noncharacteristic relation [Eq. (16)] from the sum of the finite-difference forms of Eq. (13) evaluated for $\theta=0$ and $\theta=\pi/2$. The resulting compatibility equations do not contain cross derivatives at the solution point [i.e., all terms containing $\partial u_i/\partial x_j(6)$ are eliminated]. These five finite-difference equations are solved using Gauss elimination to obtain the five dependent flow properties at the solution point. For the predictor, the flow property values at the solution point appearing in the coefficients of the derivatives in the set of difference equations are equated to those at point 5. For the corrector, the flow property values at point 6 obtained on the previous iteration are used. The resulting scheme has second-order accuracy[8] and does not violate the domain of dependence at the solution point.

The unit process to obtain the solution at a solid boundary point is almost identical to the interior point unit process. Here, however, both points 5 and 6 are constrained to lie on the solid boundary. Moreover, point 4 corresponding to the bicharacteristic with $\theta=3\pi/2$ is not inside the flowfield so the corresponding compatibility relation is not employed. That equation is replaced by the flow tangency condition

$$u_i(6)n_{bi}(6)=0 \tag{21}$$

where $n_{bi}(6)$ $(i=1,2,3)$ is the unit normal to the solid boundary at point 6.

Bow Shock Wave Point Unit Process

The bow shock wave point scheme is a predictor-corrector algorithm, with the corrector being generally iterated to convergence. Unlike the interior or solid boundary point unit processes, achievement of second-order accuracy in this scheme requires the use of field point data in the solution plane. Consequently, a global iteration process must be used.

Figure 3 depicts the bow shock wave point computational network. The intersection of the shock wave with the initial-value plane and the solution plane defines curves A and B, respectively. The solution point, at which the upstream properties are known, is denoted by point 2. A rearward-running bicharacteristic is extended from point 2 to the initial-value plane, intersecting this plane at point 1. Point 3 is an adjacent interior point used to define the meridional plane of point 2. Point 4 is the intersection of curve A with the meridional plane of point 2.

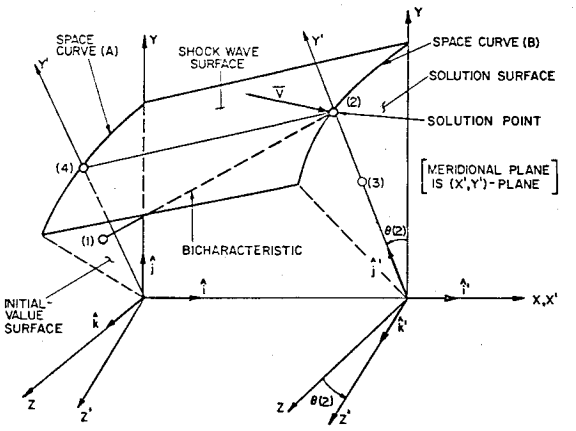

Fig. 3 Bow shock wave point computational network.

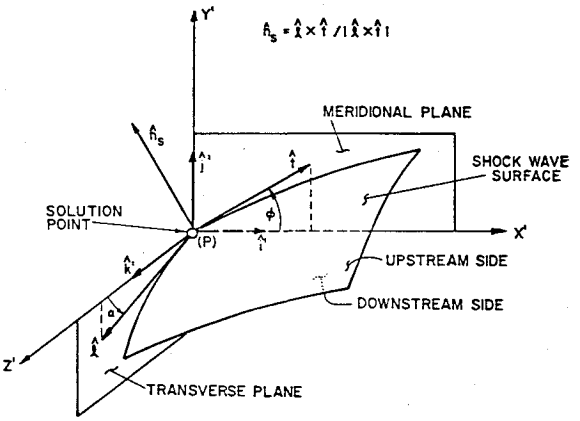

Fig. 4 Shock wave surface unit vectors.

A local Cartesian coordinate system (x',y',z') is used to describe the orientation of the shock wave surface. The coordinate x' is coincident with the x axis, y' is in the radial direction through point 2, and z' is normal to the (x',y') plane. As shown in Fig. 4, the local shock wave surface orientation at a point P is described by the set of three unit vectors: n_s, ℓ, and t. The vector n_s is normal to the shock wave surface at point P. The vector t is tangent to the shock wave at point P, lies in the meridional plane of that point, and subtends an angle ϕ with the x' axis. The vector ℓ is tangent to the shock wave at point P, lies in the transverse plane, and subtends an angle α with the z' axis. Expressions for the three unit vectors are given by

$$t=\cos\phi i'+\sin\phi j' \tag{22}$$

$$\ell=\sin\alpha j'+\cos\alpha k' \tag{23}$$

$$n_s=\ell\times t/|\ell\times t| \tag{24}$$

The shock wave point unit process is initiated by locating the solution point. The solution point is arbitrarily selected to lie in the meridional plane of point 3. The radial position of the solution point is obtained from

$$r(2)=r(4)+[x(2)-x(4)]\tan\{\tfrac{1}{2}[\phi(2)+\phi(4)]\} \tag{25}$$

where on the initial application of this equation, $\phi(2)$ is equated to $\phi(4)$. At point 4, $r(4)$ and $\phi(4)$ are determined by interpolation using quadratic polynomials written in terms of the polar angle $\theta=\tan^{-1}(z/y)$.

At this stage, the shock wave normal unit vector n_s at the solution point is found by using Eq. (24). The tangential unit vectors t and ℓ are obtained by use of the current values of $\phi(2)$ and $\alpha(2)$ in Eqs. (22) and (23), respectively. The value of $\alpha(2)$

is determined from

$$\alpha(2) = \tan^{-1}\left[\frac{1}{r}\frac{dr}{d\theta}\right]\Big|_{\theta(2)} \tag{26}$$

where, for the predictor, the analytical form of $r(\theta)$ used in this equation is obtained by curve-fitting points along curve A, whereas, for the global corrector, $r(\theta)$ is obtained by curve-fitting points along curve B.

The local Hugoniot relations are then applied at point 2 to obtain the downstream flow properties $u(2)$, $v(2)$, $w(2)$, $P(2)$, and $\rho(2)$. Next, a rearward-running bicharacteristic is extended from the solution point back to the initial-value plane, intersecting this plane at point 1. The coordinates of point 1 are obtained using a finite-difference form of Eq. (11) evaluated for the parametric angle of $\theta=\pi/2$. The flow properties at point 1 are obtained by interpolation using Eq. (19).

At this stage, the wave surface compatibility equation corresponding to the parametric angle $\theta=\pi/2$ is applied between points 1 and 2. The appropriate equation is obtained by writing Eq. (13) evaluated for $\theta=\pi/2$ in finite-difference form and solving for the pressure at point 2. Denote this pressure as $P^*(2)$. The resulting equation contains cross derivatives (terms containing $\partial u_i/\partial x_j$ which represent differentiation in the wave surface but normal to the bicharacteristic direction) at both points 1 and 2. For the predictor, the cross derivatives at point 2 are equated to those at point 1. For the global corrector, the cross derivatives at point 2 are evaluated at that point by analytically differentiating interpolation polynomials fit in the solution plane.

The pressure $P(2)$ is calculated from the local Hugoniot equations, whereas the pressure $P^*(2)$ is calculated from the wave surface compatibility relation. The difference between $P(2)$ and $P^*(2)$ is driven to within a specified tolerance of zero using the secant method with iteration being performed on the shock wave angle $\phi(2)$.

The shock wave point unit process is first applied as a predictor for each shock wave solution point. In this application, the value of α used in Eq. (23) is obtained by curve-fitting points along curve A, and the cross derivatives at point 2 are equated to those at point 1. After a predicted solution has been obtained at each shock wave point, a number of ensuing global corrections are performed. Here, the value of α used in Eq. (23) is based upon data along curve B, and the cross-derivative terms at the solution point are evaluated at that point. The resulting algorithm has second-order accuracy when the global correction is performed. The global iteration is terminated when successive values of α have converged at each of the shock wave solution points.

Solid Body-Shock Wave Point Unit Process

This unit process is used to obtain the flow properties downstream of the shock wave at a point where the shock wave intersects a solid boundary. The computational network used in this scheme is depicted in Fig. 5 where a typical solution point is denoted by point P. The intersections of the shock wave with the solid boundary and the meridional plane passing through point P define space curves A and B, respectively. The unit vectors tangent to space curves A and B at point P are denoted by ℓ and t, respectively. The unit vectors normal to the shock wave and the solid boundary at point P are denoted by n_s and n_b, respectively.

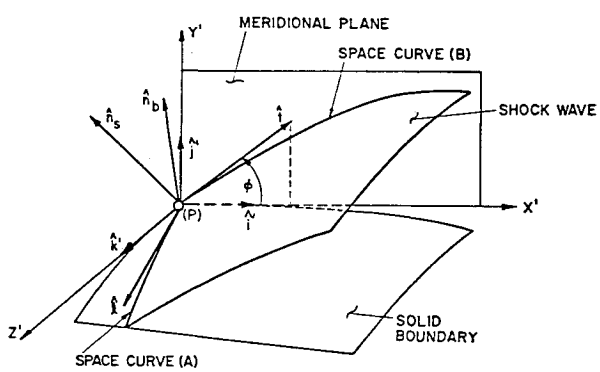

Fig. 5 Solid body-shock wave point computational network.

As for the bow shock wave point unit process, the vectors ℓ, t, and n_s are referenced to the local coordinate system (x',y',z'), where x', y', and z' have the same definitions as noted before. The tangential unit vector t again lies in the meridional plane and is defined by Eq. (22). The tangential unit vector ℓ along curve A is defined by

$$\ell = \frac{dx'}{ds}i' + \frac{dy'}{ds}j' + \frac{dz'}{ds}k' \tag{27}$$

where ds denotes the differential arc length along space curve A.

The solid body-shock wave point unit process is initiated by determining the unit vectors n_b and ℓ. An assumption is then made for the angle ϕ in Eq. (22), and the unit vector n_s is computed using Eq. (24). The local Hugoniot relations are then applied to obtain the downstream flow properties at point P. The velocity normal to the wall and downstream of the shock wave is then computed and relaxed to within a specified tolerance of zero by varying the shock wave angle ϕ using the secant iteration method.

Internal Flow Unit Processes

During the computation of the internal flow, the interior point and the solid boundary point unit processes must occasionally be applied in modified forms. Figure 6 depicts a case in which the interior point scheme must be applied in such a form. Here the solution point Mach cone intersects not only the initial-value plane but also the solid boundary and the downstream side of the internal shock wave. The bicharacteristic intersections with the initial-value plane are computed in the conventional manner. The bicharacteristic intersections with the solid boundary and the shock wave are found by an iterative technique. The solid boundary is represented as a polynomial function of the axial coordinate x. The local shock wave surface is represented as an infinite family of straight lines between two space curves, one curve being on the current initial-value plane or solid boundary and the other being on the current solution plane or solid boundary. The shock wave surface is represented by the linear

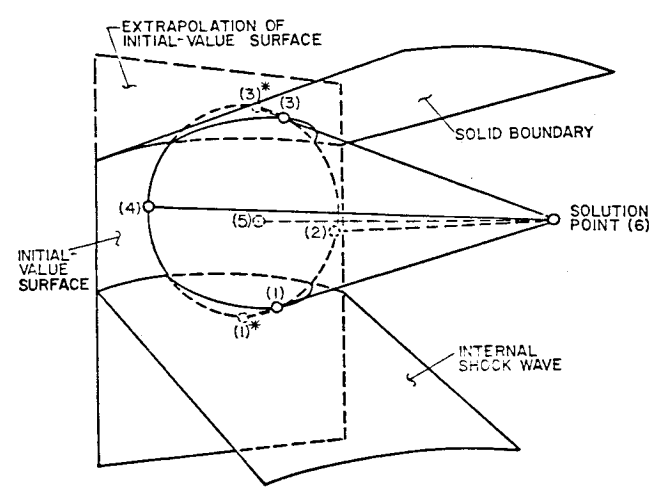

Fig. 6 Shock-modified interior point computational network.

interpolation formula

$$r(x,\theta) = \frac{(x-x_2)}{(x_1-x_2)} r_1 + \frac{(x-x_1)}{(x_2-x_1)} r_2 \tag{28}$$

where $r(x,\theta)$ is the shock wave radius at the axial position x and the polar angle $\theta = \tan^{-1}(z/y)$, x_1 and r_1 are the axial and radial positions, respectively, of the shock wave on space curve 1 at the polar angle θ, and x_2 and r_2 are the axial and radial positions, respectively, of the shock wave on space curve 2 at the polar angle θ. Quadratic curve fits in terms of θ are used to represent r_1, r_2, x_1, and x_2. Flow property values on the shock wave or on the stream surface formed by the solid boundary are found by interpolation using a quadratic trivariate polynomial of the form

$$f(x,y,z) = a_1 + a_2 y + a_3 z + a_4 yz + a_5 y^2 + a_6 z^2 + a_7 xy + a_8 xz \tag{29}$$

where the coefficients a_i $(i=1\text{-}8)$ are determined by a least squares fit of $N(N>8)$ points on either the shock wave or the solid boundary.

The unit process employed to compute the solution at a shock wave point in the internal flowfield is similar to the bow shock wave point unit process. In the internal flow shock scheme, however, the flow properties upstream of the shock wave at the solution point are determined by the application of a modified interior point unit process. Modifications to the internal flow shock wave point unit process are made when a shock wave solution point lies on or close to a solid boundary.

Shock Wave-Solid Boundary Reflections

At angle of attack, the intersection of the internal shock wave with a solid boundary forms a three-dimensional space curve. On this curve, the flow properties on the upstream and downstream sides of the incident shock wave are determined by a simultaneous solution procedure using the solid boundary point and shock wave point unit processes. The flow properties on the downstream side of the reflected shock wave are found using the solid boundary-shock wave point unit process. The flow properties downstream of the incident shock wave constitute the upstream flow properties for the reflected shock wave.

Overall Numerical Algorithm

The external flow about the forebody is computed first. The external flowfield integration requires the periodic addition of streamlines in order to retain a well-dispersed computational mesh. Furthermore, periodic deletion of selected streamlines is required so that the number of computational points lies within specified bounds.

The internal flowfield can be computed with or without the discrete fitting of the internal shock wave system. The option in which shock waves are not discretely fitted may be used in cases in which the internal shock waves are quite weak in strength, and thereby an acceptable solution can be obtained by smearing the internal discontinuities.

Initial Data and Boundary Conditions

The initial data are specified on a plane of constant x. The flow must be supersonic at each point on this plane. Many supersonic mixed-compression inlets employ a centerbody whose initial contour is conical. The initial data for the flow about a circular cone at incidence may be obtained by employing the results of Jones.[11]

The computer program developed in the present study accepts axisymmetric centerbody and cowl contours. The body radius may be described either by tabular input or through the use of cubic splines. More arbitrary geometries can be readily incorporated into the program by replacement of the existing geometry module.

Integration Step Size Regulation

Except in the vicinity of an intersection of the internal shock wave with a solid boundary, the axial marching step between successive solution planes is determined by the application of the Courant-Friedrichs-Lewy (CFL) stability criterion.[10] The CFL stability criterion mandates that the domain of dependence of the differential equations be contained within the convex hull of the finite-difference network. That is, the Mach cone must be inside the outer periphery of the nine initial-value plane field points used in formulating the bivariate interpolation polynomial [Eq. (19)].

In the vicinity of an intersection of the internal shock wave with a solid boundary, the axial step is controlled by the constraint that the shock wave-solid body intersection is contained entirely between two adjacent solution planes. The fit point stencils used in formulating the various interpolation polynomials are appropriately expanded in this case, so that the CFL stability criterion is satisfied.

Numerical Stability

A stability analysis of the nonlinear finite-difference equations for steady three-dimensional flow accounting for discrete shock wave fitting and molecular transport was not attempted. Instead, a stability analysis of the method of characteristics for steady three-dimensional isentropic flow was conducted. Stability of the generalized analysis was then verified by actual numerical calculations.

Ransom, Hoffman, and Thompson[8] conducted a von Neumann linear stability analysis of the basic interior point scheme. That analysis indicated that interpolated flow properties, instead of the actual values, should be used at the streamline-initial-value plane intersection point (point 5 in Fig. 2). The present analysis uses interpolated flow properties at all points in the initial-value plane.

Numerical Results

Some internal flow results are now presented to illustrate the capabilities of the computer program. Internal flow calculations were performed for the Boeing Mach 3.5 supersonic mixed-compression inlet described by Syberg and Hickcox.[12] This inlet has a forebody which is conical. Consequently, all of the numerical solutions were started at the cowl lip axial station. The required initial data were obtained by employing the results of Jones.[11] The assumed thermodynamic model was that of a thermally and calorically perfect gas.

Extensive boundary-layer removal is employed in this inlet to control boundary-layer separation in regions of strong adverse pressure gradients such as those caused by oblique shock wave-boundary-layer interactions. Since the present analysis does not compute the boundary layer nor takes account of boundary-layer bleed, good agreement between computed and experimental results cannot be expected in regions of high viscous interaction. For this inlet, 13.3% of the cowl lip mass flow rate was removed through boundary-layer bleed at the design point condition to control boundary-layer separation.[12]

Figure 7 presents the pressure ratio P/P_{T_∞} (static/freestream stagnation) vs the distance ratio x/R_c (axial position/cowl lip radius) for the design point condition of $M_\infty = 3.5$, zero centerbody translation, and zero angle of attack ($\alpha = 0$ deg) for three cases: 1) the two-dimensional method of characteristics program of Anderson et al.[13] with 50 radial points across the annulus, 2) the present method with 11 radial points, and 3) the present method with 21 radial points. For the case with 11 radial stations, good overall agreement is observed. A slight smearing downstream of the second in-

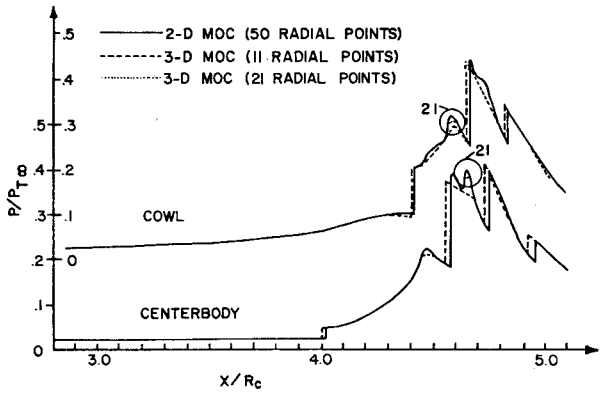

Fig. 7 Comparison of two- and three-dimensional method of characteristics results for design point.

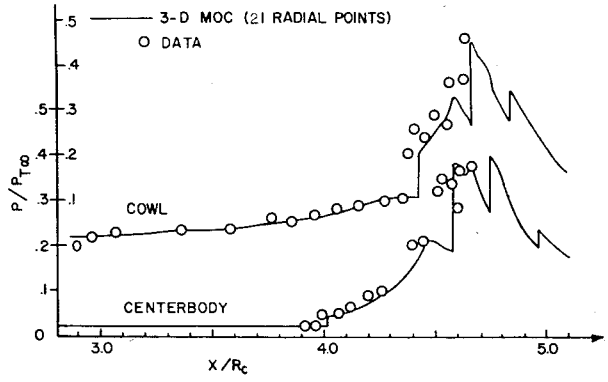

Fig. 8 Comparison of computed results with experiment for design point.

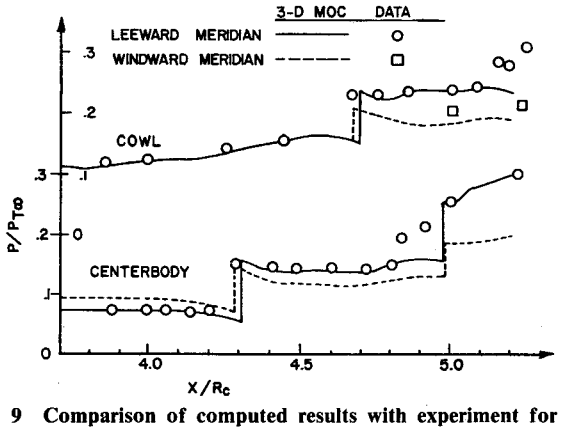

Fig. 9 Comparison of computed results with experiment for off-design case 1.

tersection of the shock wave with the centerbody and a shifting of the locations of the shock wave-solid boundary intersections are present. For the case with 21 radial stations, the agreement is excellent. The only differences are in the regions enclosed by the circles. Comparisons of numerical results with experimental data are shown in Fig. 8. Generally speaking, good agreement is observed with the best agreement being obtained away from the regions of boundary-layer removal.

For off-design operation, the centerbody must be translated forward as the angle of attack is increased or as the freestream Mach number is reduced to maintain supersonic flow through the geometric throat of the annulus. In the following discussion, the nondimensional centerbody translation is denoted by $\Delta x/R_c$.

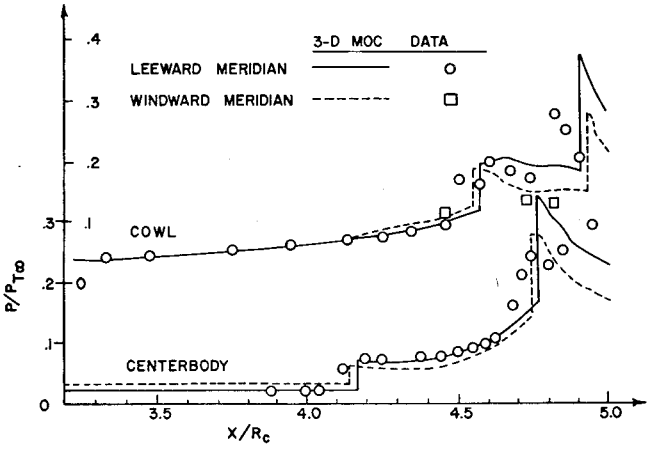

Fig. 10 Comparison of computed results with experiment for off-design case 2.

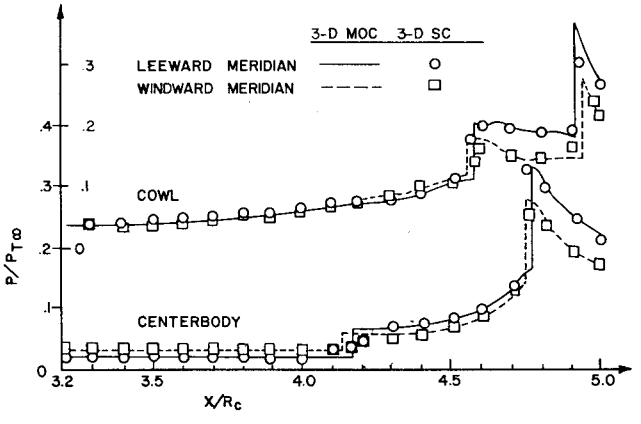

Fig. 11 Comparison of method of characteristics with shock capturing scheme for off-design case 2.

Numerical results were obtained for two off-design conditions: 1) $M_\infty = 2.5$ with a centerbody translation $\Delta x/R_c = 0.855$, and 2) $M_\infty = 3.3$ with $\Delta x/R_c = 0.356$, both for $\alpha = 3.0$ deg. For all of the computations, 21 circumferential stations and 11 radial stations were employed in the computed sector. Figure 9 presents the results for off-design case 1 for $\alpha = 3.0$ deg. Generally speaking, good overall agreement between theory and experiment is obtained except in regions of high viscous interaction and boundary-layer bleed. For this case, the maximum deviation in mass flow rate at any solution plane from the initial mass flow rate is 0.44%. The case illustrated in Fig. 9 required 46 solution planes and approximately 22 min of CPU time on a CDC-6500 computer. This yields a computation rate of about 8 points/s on this machine.

Figure 10 presents the results for off-design case 2 for $\alpha = 3.0$ deg. Fairly good overall agreement between the analysis and experiment is obtained until regions of high viscous interaction and boundary-layer removal are reached. For this case, the maximum deviation of the mass flow rate at any solution plane is 0.67%.

The present method was compared to the shock-capturing method developed by Presley.[14] That method employs the second-order accurate MacCormack finite-difference operator.[15] Figure 11 compares the pressure distributions given by the method of characteristics scheme to those given by the shock-capturing technique for the case of $M_\infty = 3.3$, $\alpha = 3.0$ deg, and $\Delta x/R_c = 0.356$. The shock-capturing algorithm employed 11 circumferential stations and 21 radial stations. For the most part, good agreement between the two analyses is obtained. In the method of characteristics

solution, however, the shock wave-solid boundary intersections are more sharply defined. This effect is to be expected, since in the shock-capturing technique shock waves are not discretely fitted but rather are smeared over a number of mesh points.

Conclusions

A number of conclusions concerning the present analysis can be made:

1) For axisymmetric flows, the solution obtained by the present analysis agrees well with the solution obtained by the two-dimensional method of characteristics.

2) Except in the regions of strong viscous interaction and boundary-layer removal, the results of the present analysis agree well with experimental data.

3) Good agreement is obtained between the present analysis and a finite-difference shock-capturing technique for three-dimensional flow solutions. However, the present analysis, which discretely fits shock waves, provides a better resolution of the shock wave structure.

Acknowledgment

This work was sponsored by the NASA Lewis Research Center under Grants NGR-15-005-162 and NGR-15-005-191.

References

[1] Vadyak, J., "The Flow Field Calculation in Supersonic Mixed-Compression Aircraft Inlets at Angle of Attack Using the Three-Dimensional Method of Characteristics with Discrete Shock Wave Fitting," Ph.D. Thesis, Purdue Univ., West Lafayette, Ind., Dec. 1977.

[2] Ferri, A. and Dash, S., "Viscous Flow at High Mach Numbers with Pressure Gradients," *Proceedings of 1969 Symposium on Viscous Interaction Phenomena in Supersonic and Hypersonic Flow,* University of Dayton Press, Dayton, Ohio, 1970.

[3] Richtmyer, R. D. and Morton, K. W., *Difference Methods for Initial-Value Problems,* Interscience Publishers, New York, N. Y., 1967, p. 378.

[4] Moretti, G., "Thoughts and Afterthoughts about Shock Computations," Polytechnic Institute of Brooklyn, PIBAL Rept. 72-37, Dec. 1972.

[5] Salas, M. D., "Shock Fitting Method for Complicated Two-Dimensional Supersonic Flows," *AIAA Journal,* Vol. 14, May 1976, pp. 583-588.

[6] Butler, D. S., "The Numerical Solution of Hyperbolic Systems of Partial Differential Equations in Three Independent Variables," *Proceedings of Royal Society of London,* Vol. A255, 1960, pp. 232-252.

[7] Rusanov, V. V., "The Characteristics of General Equations of Gas Dynamics," *Zhurnal Vychistlitel'Noi Matematiki,* Vol. 3, No. 3, 1963, pp. 508-527.

[8] Ransom, V. H., Hoffman, J. D., and Thompson, H. D., "A Second-Order Numerical Method of Characteristics for Three-Dimensional Supersonic Flow, Vol. I, Theoretical Development and Results," Air Force Aero Propulsion Laboratory, Wright-Patterson Air Force Base, Ohio, Rept. AFAPL-TR-69-98, Oct. 1969.

[9] Cline, M. C. and Hoffman, J. D., "The Analysis of Nonequilibrium, Chemically Reacting, Supersonic Flow in Three-Dimensions, Vol. I, Theoretical Development and Results," Air Force Aero Propulsion Laboratory, Wright-Patterson Air Force Base, Ohio, Rept. AFAPL-TR-71-73, Aug. 1971.

[10] Courant, R., Friedrichs, K. O., and Lewy, H., "Uber die Partiellen Differenzialgleichungen der Mathematischen Physik," *Mathematische Annalen,* Vol. 100, 1928, pp. 32-74.

[11] Jones, D. J., "Numerical Solutions of the Flow Field for Conical Bodies in a Supersonic Stream," National Research Council of Canada, Rept. LR-507, 1968.

[12] Syberg, J., and Hickcox, T. E., "Design of a Bleed System for a Mach 3.5 Inlet," NASA CR-2187, 1973.

[13] Anderson, B. H., Tassa, Y., and Reshotko, E., "Characteristic Procedure for Supersonic Flows Including Consideration of Viscous Contributions to Flow Rotationality," AIAA Paper 76-426, 1976.

[14] Presley, L. L., "Internal Flow Calculations for Axisymmetric Supersonic Inlets at Angle of Attack," AIAA Paper 75-1214, 1975.

[15] MacCormack, R. W., "The Effect of Viscosity in Hypervelocity Impact Cratering," AIAA Paper 69-354, 1969.

U.S. POSTAL SERVICE
STATEMENT OF OWNERSHIP, MANAGEMENT AND CIRCULATION
(Required by 39 U.S.C. 3685)

1. TITLE OF PUBLICATION	A. PUBLICATION NO.	2. DATE OF FILING
AIAA JOURNAL	0 0 9 9 2 0	Oct. 1,1980
3. FREQUENCY OF ISSUE	A. NO. OF ISSUES PUBLISHED ANNUALLY	B. ANNUAL SUBSCRIPTION PRICE
MONTHLY	12	$10.00

4. LOCATION OF KNOWN OFFICE OF PUBLICATION (Street, City, County, State and ZIP Code) (Not printers)
1290 AVENUE OF THE AMERICAS, NEW YORK, N.Y. 10104

5. LOCATION OF THE HEADQUARTERS OR GENERAL BUSINESS OFFICES OF THE PUBLISHERS (Not printers)
SAME AS ABOVE

6. NAMES AND COMPLETE ADDRESSES OF PUBLISHER, EDITOR, AND MANAGING EDITOR

PUBLISHER (Name and Address)
AMERICAN INSTITUTE OF AERONAUTICS AND ASTRONAUTICS, INC., SAME AS ABOVE

EDITOR (Name and Address)
GEORGE W. SUTTON SAME AS ABOVE

MANAGING EDITOR (Name and Address)
ELAINE J. CAMHI SAME AS ABOVE

7. OWNER (If owned by a corporation, its name and address must be stated and also immediately thereunder the names and addresses of stockholders owning or holding 1 percent or more of total amount of stock. If not owned by a corporation, the names and addresses of the individual owners must be given. If owned by a partnership or other unincorporated firm, its name and address, as well as that of each individual must be given. If the publication is published by a nonprofit organization, its name and address must be stated.)

NAME	ADDRESS
AMERICAN INSTITUTE OF AERONAUTICS AND ASTRONAUTICS, INC.	SAME AS ABOVE

8. KNOWN BONDHOLDERS, MORTGAGEES, AND OTHER SECURITY HOLDERS OWNING OR HOLDING 1 PERCENT OR MORE OF TOTAL AMOUNT OF BONDS, MORTGAGES OR OTHER SECURITIES (If there are none, so state)

NAME	ADDRESS
NONE	

9. FOR COMPLETION BY NONPROFIT ORGANIZATIONS AUTHORIZED TO MAIL AT SPECIAL RATES (Section 132.122, PSM)
The purpose, function, and nonprofit status of this organization and the exempt status for Federal income tax purposes (Check one)
☐ HAVE NOT CHANGED DURING PRECEDING 12 MONTHS ☐ HAVE CHANGED DURING PRECEDING 12 MONTHS (If changed, publisher must submit explanation of change with this statement.)

10. EXTENT AND NATURE OF CIRCULATION	AVERAGE NO. COPIES EACH ISSUE DURING PRECEDING 12 MONTHS	ACTUAL NO. COPIES OF SINGLE ISSUE PUBLISHED NEAREST TO FILING DATE
A. TOTAL NO. COPIES PRINTED (Net Press Run)	5925	4800
B. PAID CIRCULATION 1. SALES THROUGH DEALERS AND CARRIERS, STREET VENDORS AND COUNTER SALES	----	----
2. MAIL SUBSCRIPTIONS	5321	4444
C. TOTAL PAID CIRCULATION (Sum of 10B1 and 10B2)	5321	4444
D. FREE DISTRIBUTION BY MAIL, CARRIER OR OTHER MEANS SAMPLES, COMPLIMENTARY, AND OTHER FREE COPIES	41	51
E. TOTAL DISTRIBUTION (Sum of C and D)	5362	4500
F. COPIES NOT DISTRIBUTED 1. OFFICE USE, LEFT OVER, UNACCOUNTED, SPOILED AFTER PRINTING	563	300
2. RETURNS FROM NEWS AGENTS	----	----
G. TOTAL (Sum of E, F1 and 2—should equal net press run shown in A)	5925	4800

11. I certify that the statements made by me above are correct and complete. SIGNATURE AND TITLE OF EDITOR, PUBLISHER, BUSINESS MANAGER, OR OWNER
Nelson W. Friedman, Admin., Mgmt. Sys.

12. FOR COMPLETION BY PUBLISHERS MAILING AT THE REGULAR RATES (Section 132.121, Postal Service Manual)
39 U. S. C. 3626 provides in pertinent part: "No person who would have been entitled to mail matter under former section 4359 of this title shall mail such matter at the rates provided under this subsection unless he files annually with the Postal Service a written request for permission to mail matter at such rates."
In accordance with the provisions of this statute, I hereby request permission to mail the publication named in Item 1 at the phased postage rates presently authorized by 39 U. S. C. 3626.
SIGNATURE AND TITLE OF EDITOR, PUBLISHER, BUSINESS MANAGER, OR OWNER
Nelson W. Friedman, Administrator, Management Systems